Click here to view PowerPoint presentation; Press Esc to exit

Theoretical and Observational Studies of Meteor Interactions with the Ionosphere

P. Colestock, S. Close and John Zinn
Los Alamos National Laboratory, Space and Remote Sensing Sciences
PO Box 1663
Los Alamos, NM
USA

ABSTRACT

An intense flux of small-mass meteors has been seen in large-aperture radar scattering for many years. At high altitudes, these meteoroids routinely damage orbiting satellites by both direct impact as well as spacecraft charging. This flux is believed to make up the major portion of mass flux from space. At lower altitudes, meteoroids affect ionospheric and thermospheric processes by depositing heavy metallic atoms, ions and dust. Preliminary analysis of meteors has shown that meteoroids can disrupt and halt radio communication by creating plasma density structures that are several orders of magnitude greater than those seen in the background ionosphere. To understand this phenomenon better, we have undertaken a theoretical and an observational campaign that is designed to determine empirically the mass flux coupled with a detailed plasma expansion model of the ablating material as the meteors disintegrate in the ionosphere. We will discuss our findings to date as well as our expected future program development in this area.

Key Words: Meteors; Meteoroids; Meteor Ablation; Ionospheric Metals

1.0 INTRODUCTION

For many years, the existence of metallic layers in the lower ionosphere has been known and attributed to the influx of meteors that are completely ablated in the ionosphere [Opik, 1953, Lebedinets, 1973, Zinn, 2003, Hunt 2004, ReVelle, 2005]. The metals provide unique optical signatures and have been subsequently studied extensively with respect to dynamics and how they modify the chemistry of the ionosphere under varying conditions [refs.]. However, the precise nature of the input flux is not precisely known, either in the magnitude and velocity distribution of the flux incident from extraterrestrial sources, or in the mechanisms that govern the deposition of material as a function of altitude. Deposition from the flux of larger meteoroids, such as the Leonids, [Zinn, 2003] has received some attention, however recent radar measurements indicate the bulk of material deposited in the ionosphere originates from a large flux of micro-meteoroids, for which an appropriate deposition model has not yet been formulated. Moreover, the formation and expansion of the plasma plume about micro-meteoroids forms the primary means by which we can remotely sense the mass and velocity distribution associated with this flux. Previous work has shown that there is some ambiguity regarding the interpretation of radar scattering data in determining the flux distribution parameters. This information is not only important for the understanding of ionospheric composition, but also to assess the potential damage to spacecraft and effects on space-based remote sensing.

In order to better understand this phenomenon, we undertake in this work an assessment of the processes affecting meteoroid ablation and the formation and evolution of the ablation-produced plasma plume.

Colestock, P.; Close, S.; Zinn, J. (2006) Theoretical and Observational Studies of Meteor Interactions with the Ionosphere. In *Characterising the Ionosphere* (pp. 12-1 – 12-12). Meeting Proceedings RTO-MP-IST-056, Paper 12. Neuilly-sur-Seine, France: RTO. Available from: http://www.rto.nato.int/abstracts.asp.

Report Documentation Page

Form Approved
OMB No. 0704-0188

1. REPORT DATE	2. REPORT TYPE	3. DATES COVERED
01 JUN 2006	**N/A**	**-**

4. TITLE AND SUBTITLE	5a. CONTRACT NUMBER
Theoretical and Observational Studies of Meteor Interactions with the Ionosphere	5b. GRANT NUMBER
	5c. PROGRAM ELEMENT NUMBER
6. AUTHOR(S)	5d. PROJECT NUMBER
	5e. TASK NUMBER
	5f. WORK UNIT NUMBER
7. PERFORMING ORGANIZATION NAME(S) AND ADDRESS(ES) **Los Alamos National Laboratory, Space and Remote Sensing Sciences PO Box 1663 Los Alamos, NM USA**	8. PERFORMING ORGANIZATION REPORT NUMBER
9. SPONSORING/MONITORING AGENCY NAME(S) AND ADDRESS(ES)	10. SPONSOR/MONITOR'S ACRONYM(S)
	11. SPONSOR/MONITOR'S REPORT NUMBER(S)

12. DISTRIBUTION/AVAILABILITY STATEMENT
Approved for public release, distribution unlimited

13. SUPPLEMENTARY NOTES
See also ADM002065., The original document contains color images.

14. ABSTRACT

15. SUBJECT TERMS

16. SECURITY CLASSIFICATION OF:			17. LIMITATION OF ABSTRACT	18. NUMBER OF PAGES	19a. NAME OF RESPONSIBLE PERSON
a. REPORT	b. ABSTRACT	c. THIS PAGE			
unclassified	**unclassified**	**unclassified**	**UU**	**30**	

In section 2, we review the radar-based measurements of the meteor flux, and in section 3 we calculate the inferred velocity magnitude and mass distribution. In section 4 we present a model for meteor ablation and compute estimated deposition profiles. In section 5 we discuss the related problem of determining the self-consistent plasma plume which is created by the ablating material, and discuss its structure as a function of altitude. Section 6 is a summary of our results and plans for future study of this area.

2.0 METEOR FLUX MEASUREMENTS

One of the most pressing and debated topics in the field of meteoroid physics concerns the meteoroid mass flux. Specifically, the amount of material (i.e. the mass flux) impacting Earth every year has yet to be conclusively determined and estimates vary by as much as two orders of magnitude. This discrepancy must be due, in part, to the various selection effects and biases inherent in every collection campaign. For instance, optical measurements tend to be biased towards the larger, brighter meteoroids, whereas high-power, large-aperture (HPLA) radars appear to be biased towards the faster meteoroids.

The yearly whole-earth mass flux, per decade of particle mass, is shown in Figure 2.1 This figure was extracted from Mathews et al. [2001] and shows a comparison between three different estimates, including Ceplecha et al. [1998], Love and Brownlee [1993] and Mathews et al. [2001]. The mass flux determination by Ceplecha et al. is based on the Grun et al. [1985] analysis of spacecraft impact results, lunar micro-cratering and Zodiacal light observations. The mass flux determined by Love and Brownlee [1993] is based on data collected by Long Duration Exposure Facility (LDEF). Love and Brownlee assumed an average particle speed of ~17 km/s with an average impact angle of 45 degrees, which results in the 12 km/s normal-to-LDEF-surface speed that they used to convert crater diameter to particle energy and finally to mass. Mathews re-derived the Love and Brownlee results using a much higher peak velocity distribution (~50 km/s), which is the detected velocity peak using Arecibo Observatory. These results are also shown in Figure 2.1. Therefore, the peak velocity distribution plays a primary role in determining mass flux and has yet to be conclusively determined.

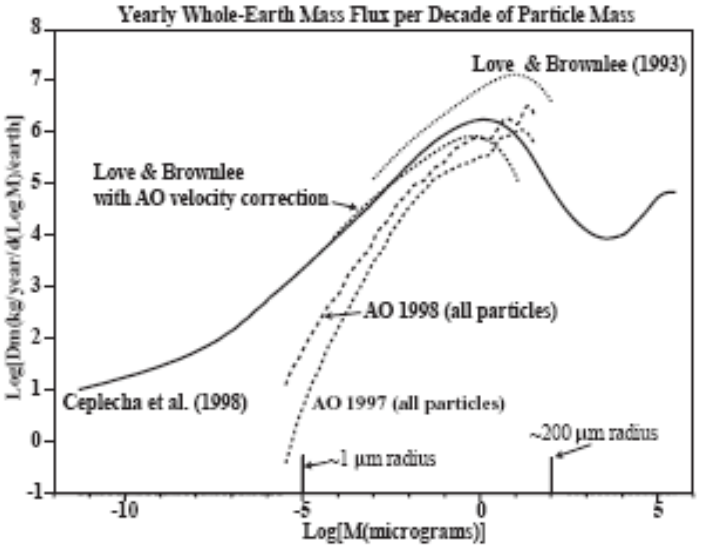

Fig. 2.1: Annualized whole earth mass flux per decade of mass, showing results from Mathews et al. [2001], Ceplecha et al. [1998], Love and Brownlee [1993]. This figure corresponds to Figure 2 in Mathews et al. [2001].

3.0 MASS DETERMINATION

We calculate the mass of a meteoroid using head echo radar-cross-section (RCS) data by applying the new technique described in Close *et al.* (2005). We refer to these masses as "scattering masses". We achieve this new result by converting measured head echo RCS to peak plasma density, and thence to electron line density, *q*, using our new spherical scattering theory described in Close *et al.* (2004). For meteor trails, *q* is constant at a given altitude. For head echoes, however, *q* depends on *r* and varies up to its maximum radius, r_{max}. We therefore use the integrated line density for subsequent use in our calculations, which is given by

$$q = 2\pi \int_0^{r_{\max}} n(r) r dr \qquad \text{Eq. 1}$$

where *n(r)* is the plasma density at radius *r* output from the spherical scattering solution. The line densities are then input into the standard meteoroid mass-loss equation to determine meteoroid mass

$$\frac{dm}{dt} = \frac{q\mu v}{\beta} \qquad \text{Eq. 2}$$

where *m* is the meteoroid mass, μ is the mean molecular mass, which is approximately 20 amu for stony meteoroids dominated by 60% oxygen and 25% silicon, *v* is the head echo 3D speed and β is the ionization probability, which depends upon the speed and scales as $4.91 \times 10^{-6} v^{2.25}$ for meteoroid velocities between 30 and 61 km/s (*Jones* 1997). Alternatively, we could use the ionization probability equation given by Lebedinets *et al.* (1973) or Bronshten (1983), however these alternatives for β typically only change the meteoroid mass by less than a factor of 5. Note that in order to obtain the scattering mass, we must estimate the meteoroid mean molecular mass, as well as the ionization probability.

In Close *et al.* (2005), we compared the scattering mass with the more-traditional "dynamical mass". The dynamical mass method, which is determined by first assuming a meteoroid density, is derived by conserving momentum between the air molecule and the meteoroid and was first proposed by Opik (1958) and subsequently applied to HPLA data collected at Arecibo by Janches *et al.* (2000) and Mathews *et al.* (2001). Upon our comparison of the two methods, we concluded that the scattering mass appears to be more physically pleasing than the dynamical mass due to the following: (1) the scattering masses always decrease as altitude decreases, contrary to dynamical masses which sometimes increase along a portion of the trajectory, (2) the scattering masses show an exponential decay consistent with atmospheric drag modeling, whereas dynamical masses often show a linear decrease, (3) the scattering masses show a trend with altitude where the highest mass meteoroids are located at the lowest altitudes as physical theory suggests, whereas the dynamical masses do not always follow this trend, and (4) most importantly, the scattering masses never give us unphysical results, such as extremely high or extremely low masses. The dynamical masses sometimes produce meteoroids with exceptionally low masses ($<10^{-12}$ grams) that are below the limit of ablation. We concluded that either fragmentation processes, errors in the velocity determination method (this would also affect the scattering mass), or ignoring higher-order terms in the conservation equation may lead to these unphysical results in the dynamical masses. We should note, however, that on average, the two methods agree to within an order of magnitude.

The histograms of scattering mass, calculated from data collected at the ALTAIR radar at 160 MHz, are contained in Figure 1. These represent the maximum mass from each head echo streak and comprise 451 VHF head echoes detected during the Leonid 1998 shower, and 223 VHF head echoes detected during

Leonid 1999 shower. For the Leonid 1998 shower, the median meteoroid mass detected at VHF is 4.52 x 10^{-6} grams; at UHF, the median mass is 1.07 x 10^{-6} grams. For the Leonid 1999 data, the median meteoroid mass detected at VHF is 1.36 x 10^{-5} grams, while the median meteoroid mass detected at UHF is 1.87 x 10^{-6} grams. These data represent a biased sample of meteoroids detected using the ALTAIR radar, since it is difficult to detect the low-mass/low-velocity population.

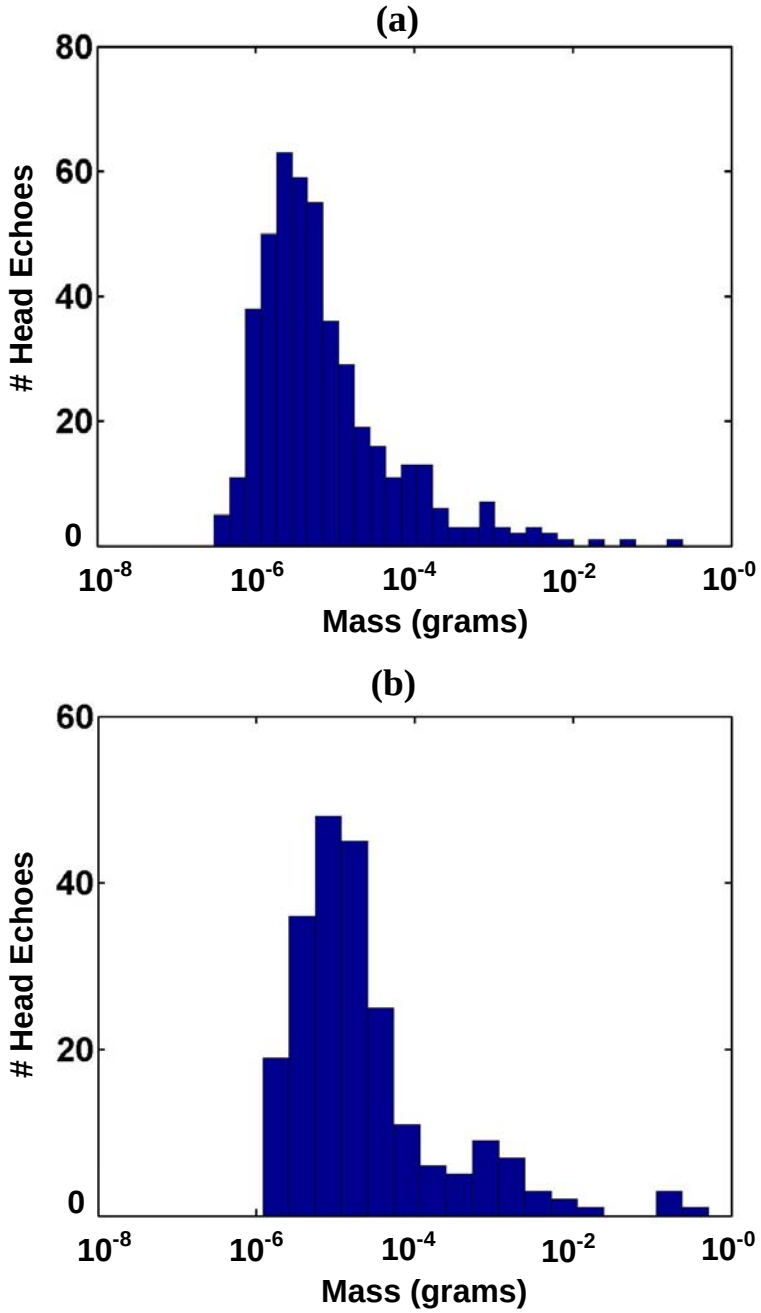

Fig. 3.1: Histogram of mass, calculated using the new scattering theory, for VHF head echo data collected during the (a) Leonid 1998 shower and (b) Leonid 1999 shower. The total number of head echoes shown is 451 and 223, respectively.

4.0 ABLATION MODEL

When a micro-meteoroid impinges upon the upper atmosphere, air molecules and atoms impact the body with a large mean energy in the range of 200-800 eV. The rate at which material is evaporated from the meteor is given by

$$\frac{dm}{dt} = -\frac{1}{2} m_{air} v_0^3 \frac{1}{E_o} S n_{air}$$

where v_0 is the incident velocity, S is the projected area of the meteor, E_0 is the heat of ablation, m_{air} is the mean mass of the air mixture, and n_{air} is the air density at a given altitude. If we define ρ_s as the mass density of the meteor and assume a spherical meteoroid, we can express the rate of mass loss per unit path length as

$$\frac{dm}{ds} = -0.6045 \left(\frac{v_0^2 m_{air} n_{air}}{E_0} \right) \left(\frac{m}{\rho_s} \right)^{2/3}$$

If we further assume the meteor impinges upon the ionosphere with a zenith angle θ, and take the air density to vary over a scale height, H, according to

$$n_{air} = n(z_0) \exp\left\{ -\frac{z - z_0}{H} \right\}$$

then the rate of mass variation with altitude is found by evaluating

$$\frac{dm}{dz} = -0.6045 \left(\frac{v_0^2 m_{air} n_{air}(z_0)}{E_0} \right) \frac{m^{2/3}}{\cos\theta} \exp\left\{ -\frac{z - z_0}{H} \right\}$$

Now if we define z_T as the terminal altitude where $m = 0$, then we have

$$z_T = z_0 + H \ln\left\{ \frac{0.6045}{3} \left(\frac{v_0^2 m_{air} n_{air}(z_0)}{E_0} \right) \frac{H}{\cos\theta} m_0^{-1/3} \right\}$$

In the above, m_0 is the initial meteor mass and we have made the implicit assumption that the velocity is nearly constant over most of the meteor's path. This expression gives us a means of calculating the mass deposition profiles. In Figure 4.1, we show the mass variation with altitude, parameterized by initial mass. It is worthwhile to note that there is some uncertainty regarding the heat of ablation E_0. We have taken a value that gives best correspondence to the measured altitudes using high-power radar scattering ($E_0 = 5 \times 10^{10}$ *erg/gram*).

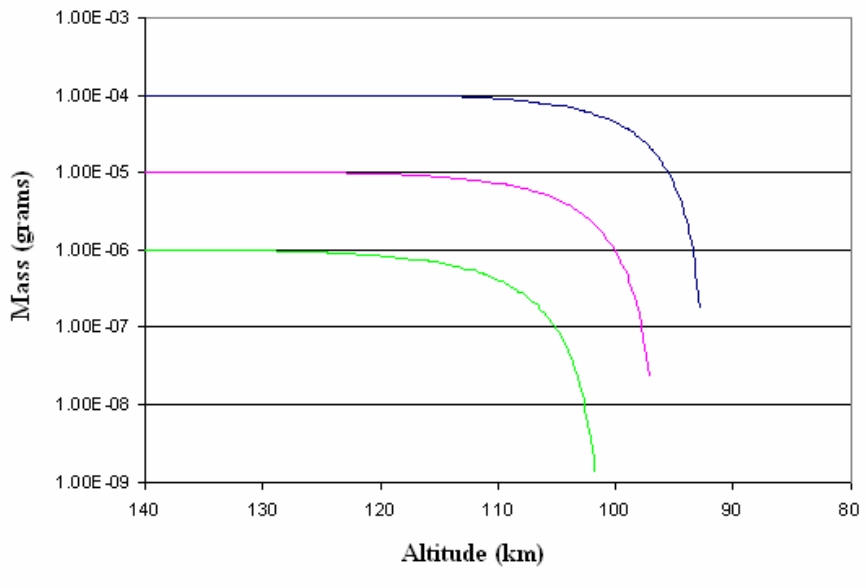

Fig. 4.1: Mass Variation with Altitude.

The corresponding mass deposition rate is shown in Fig. 4.2 for vertical incidence. We may integrate these rates over the distribution shown in Fig. 2.1 to obtain the overall mass deposition profile, as shown in Fig. 4.3. Of course, this profile will depend on the presence of any meteor storms, and its composition will vary with the sources, which are not precisely known. However, the above model will enable a separate determination of the meteoroid composition and flux based on in situ measurements of mass profiles.

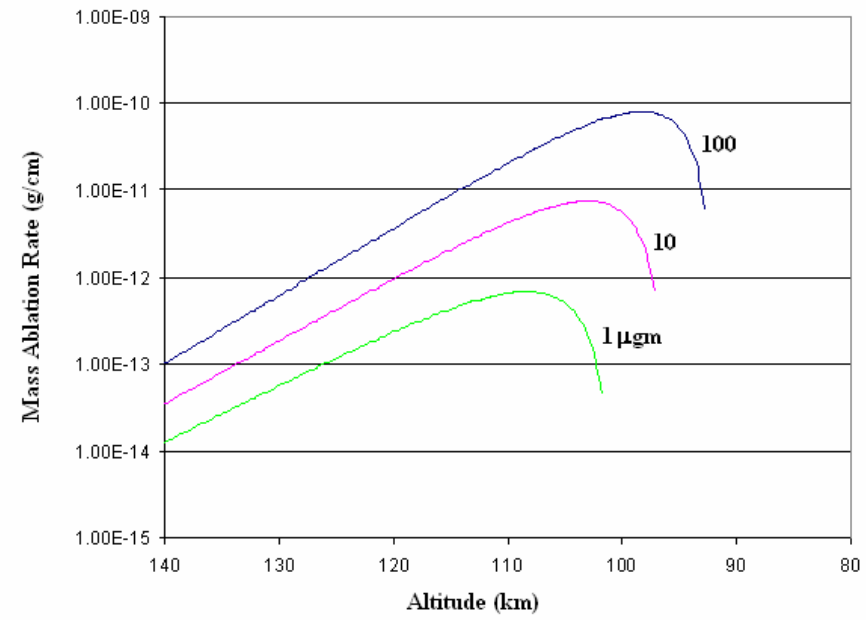

Fig. 4.2: Mass deposition profiles for 30 km/sec meteoroids as a function of initial mass.

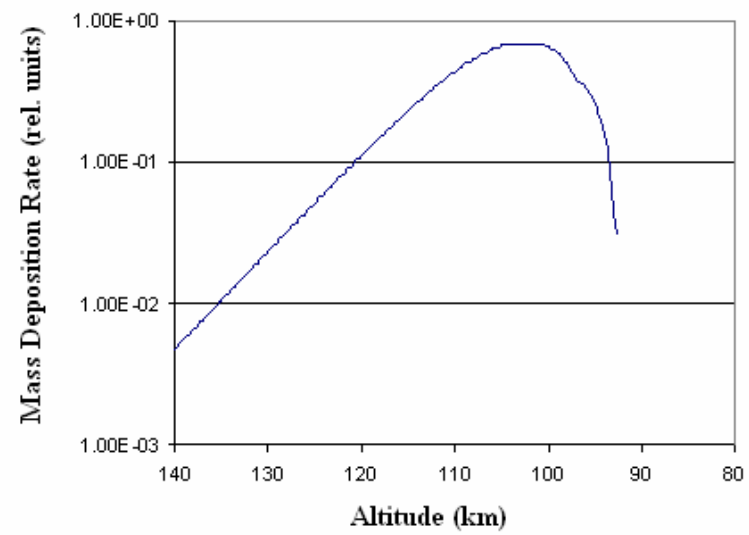

Fig. 4.3: Overall mass deposition profile based on the mass distribution shown in Fig. 2.1.

5.0 PLASMA EXPANSION MODEL

In order to assess whether this model is correct from experimental observations, we must first construct a model of the plasma plume development which represents both the radar cross-section and the source of optical emission which can be remotely sensed. As we shall see, this model is quite complex, and we are unable to give a complete treatment over all wavelengths of interest at his time. Instead we will focus here on the identification of significant mechanisms that determine the size, density and geometric configuration of the plume, leaving more detailed treatments of issues such as stability and interaction with the background ionosphere to future work. The plasma surrounding a meteor head falls into several regimes which depend on the collision rate with air molecules, hence the altitude, as shown in Fig. 4.2.

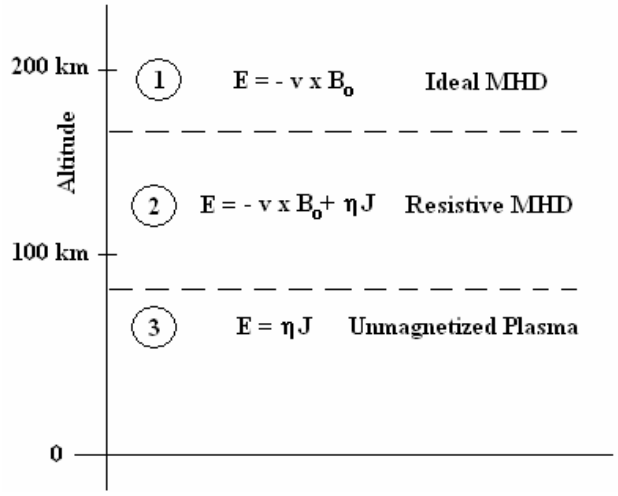

Fig 5.1: Altitude Dependence of Meteoroid Plasma Regimes.

The plume development falls into separate regimes depending on whether or not the plasma particles are magnetized in the geomagnetic field. Moreover, collisions with background neutrals determine whether the plasma exhibits significant collective effects. In region 1, there are few neutral molecules and hence little ionization. What perturbations may be created obey an Ohm's Law. This is the regime of ideal MHD, however densities are sufficiently low as to be of little practical interest. In region 2 in the figure, we have the following inequality

$$r_{meteor} << r_{Le} << l_{mfp} << r_{Li}$$

Namely, the meteor radius is much smaller than either the electron or ion Larmor radii. Moreover, the mean-free-path for electron neutral collisions is typically larger than the electron Larmor radius. In the case when collisions are sufficiently weak, namely at high altitude, plasma collective effects are important. In this case, referring to Fig. 5.1, the plasma behavior falls into separate regimes depending on the distance from the meteoroid. We see that at distances such that $r < r_{Le}$, the neither electrons nor ions are magnetized, and hence ambipolar diffusion dominates. It can be assumed that electron and ion temperatures are roughly equal, hence the electrons move more rapidly and establish an outward-pointing electric field close to the meteor.

Beyond the ambipolar region, the electrons become magnetized in the geomagnetic field (r_{Le} ~ 5 cm), but the ion Larmor radii are much larger and follow nearly straight line orbits. However, estimates of the plasma density in the bulk of the plume show that the condition

$$\omega_{pe}^2 >> \omega_{ce}^2$$

holds, which ensures that collective effects are important in this region. There are two important collective effects: first the plasma in the interface between the field-free region and the background medium experiences charge separation which causes a strong forward drift motion. Although the magnetic field strength in the background geomagnetic field is weak, a slight bending of the particle orbits in this field causes a charge separation in the $\boldsymbol{v} \times \boldsymbol{B}$ direction as shown in Fig. 5.1. The resulting *E*-field causes an $\boldsymbol{E} \times \boldsymbol{B}$ drift in the direction of the meteor motion, maintaining the plasma plume at fixed distance from the meteor. This fact is a consequence of Ohm's Law in the nearly collisionless portion of the meteor path (> 80 km).

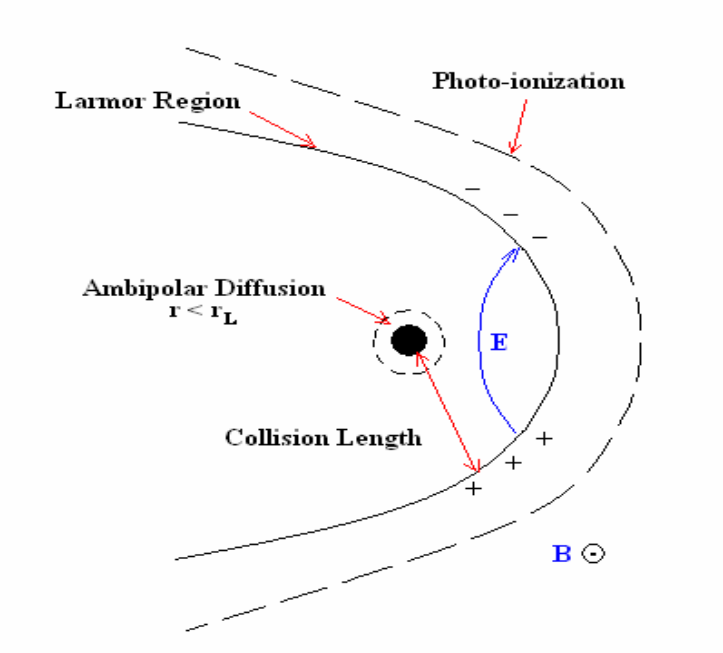

Fig. 5.1: Geometry of the Meteor Plasma Plume.

Secondly, the plasma can exhibit strong diamagnetism as it expands, creating a bubble of magnetic field-free region around the meteoroid head. The expanding material carries with it the captive field lines, resulting in a shell of plasma which carries with it ring currents that cancel the geomagnetic field, as shown in Fig. 5.2.

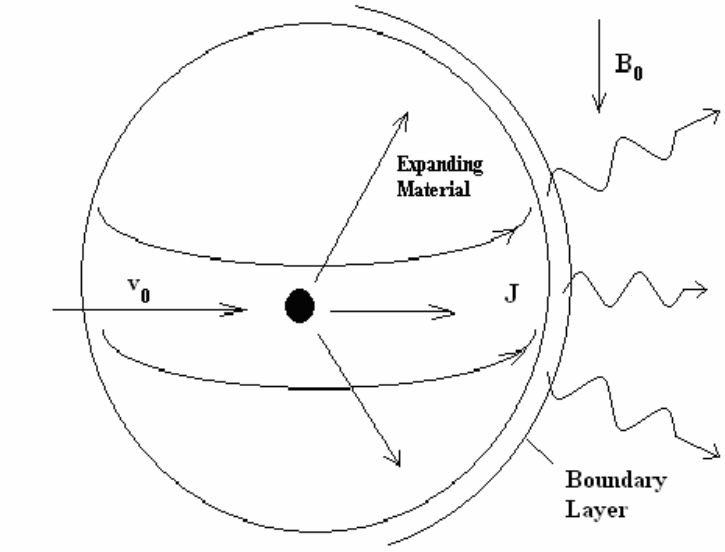

**Fig. 5.2 Diamagnetic Bubble created by Expanding Plasma.
Energetic radiation may be generated in a thin boundary layer.**

This situation has important consequences which we will describe in the following, namely the creation of a sharp boundary layer between the meteoroid plasma and the background ionospheric plasma (Longmire, 1963). Since the field lines are effectively frozen into the flow in regions 1 and 2, the ablated debris from the meteoroid leads to a strong compression of the magnetic field at the plume-background interface. For this present adaptation, we suppose that we have an unmagnetized meteor debris plasma with initial density n_d, and velocity v_0 in the x-direction. Referring to Fig. 5.2, we further assume that it is moving into a stationary magnetized air plasma, with initial density n_a, with an imbedded *B*-field in the *z* direction, with initial strength B_0. As the two plasmas interpenetrate, the magnetized electrons will move in such a way as to preserve the charge neutrality condition $n_e = n_a + n_d$. At the earliest times the ion motions are not affected by the fields, so that the debris ions continue moving with velocity v_0 and the air ions continue to be stationary. Then within the local region where the two ion populations have interpenetrated the total ion density will be $n_i \sim n_e = n_a + n_d$. The electrons are magnetized, so that the debris electrons and the air electrons do not intermix, and the air electrons carry the magnetic field with them. Therefore at some value of x within the interpenetration region there will be a sharp transition with $B = 0$ on the left and a compressed *B*-field $B = B_0 (n_a + n_d)/n_a$ in a boundary layer, as shown in Fig. 5.3.

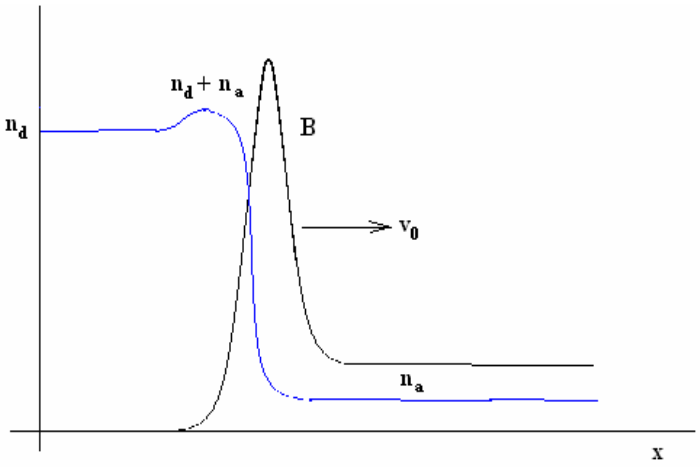

Fig. 5.3: Adiabatic Compression of the Plume Interface Due to a moving Boundary layer.

As the magnetic flux is forced over the air electrons, adiabatic compression of the orbits results which can result in rapid heating of the electrons. Essentially the $\dot{B}$ of the moving boundary layer can give rise to strong induced electric fields through transformer action, potentially producing a thin layer of energetic electrons. Ions, which are unmagnetized, will not interact significantly. Such a condition may lead to enhanced UV, or possibly even X-ray, emission from this surface. Although no such emission has been observed thus far (Jenniskens, 2002), it may well be that the dominant optical emission component that has been detected is generated by the bulk plasma which is evidently at relatively low temperature ($4.4\times10^3 K$). The boundary layer is not optically thick enough to produce large numbers of energetic photons. However, it may be noted that there is some evidence that cometary fragments can produce a small amount of energetic radiation that could be explained by such a process. (Lisse, 1996)

We note further that near the edge of the plume, the electric field drops as the plasma density decreases, producing a slower ***E x B*** velocity than that required to maintain the meteor speed, hence there is slippage of

the plasma along the plume surface. Moreover, there is drag created by collisions with neutrals that tends to amplify the slippage. In addition, the above mentioned radiation from the hot plasma in front of the meteor aids in pre-ionizing the incoming neutrals in the region beyond the plume boundary. None of these effects have been included in the present model.

6.0 SUMMARY AND FUTURE WORK

In this work we have explored various mechanisms that govern the deposition of material from meteoroids in the ionosphere. We find analytic expressions for the rate of material ablation, and couple this result with measurements of mass flux to determine overall deposition profiles. In addition we have explored mechanisms that determine the size and shape of the plasma plume surrounding the meteoroid, which should enable a better determination of meteoroid parameters with optical and radar measurements. We found that the plasma plume can be characterized in three distinct regimes: ideal MHD, non-ideal, or resistive MHD, and resistive. In each regime, collective plasma effects play a role in shaping the plume profiles.

However, much remains to be done in making these simplified models more realistic. For instance, the inclusion of a more precise ablation model, the process of collisional ionization and thermalization along with radiation transport would be required to provide a more accurate ionization profile in and around the plasma plume. In addition, we have not addressed the issue of plume stability, which could well play a key role in determining plasma parameters by remote sensing techniques. Our goal is to develop such a model both with analytic methods and numerical simulations.

Acknowledgements: We acknowledge helpful discussions with Meers Oppenheim, Doug Revelle and Ronald Kashuba during portions of this work.

REFERENCES

Bronshten, A. V., 1983. Physics of meteoric phenomena. Reidel, Dordrecht.

Ceplecha, Z., J. Borovicka, W. G. Elford, D. O. Revelle, R.L. Hawkes, V. Porubcan, and M. Simek, 1998. Meteor phenomena and bodies. Space Sci. Rev., 85, 327-471.

Close, S., M. Oppenheim, D. Durand and L. Dyrud, 2005. A new method of determining meteoroid mass from head echo data. JGR, 110.

Close, S., M. Oppenheim, S. Hunt, and A. Coster, 2004. A technique for calculating meteor plasma density and meteoroid mass from radar head echo scattering. Icarus 168, 43-52.

Hunt, S. M., Oppenheim, M., Close, S. M., Brown, P. G. McKeen, F., and Minardi, M. Determination of the Meteoroid Velocity Distribution at the Earth using High-gain Radar, Icarus, 168, 34-42.

Janches, D. J., J. D. Mathews, D. D. Meisel, and Q. Zhou, 2000. Micrometeor observations using the Arecibo 430 MHz Radar. Icarus 145, 53-63.

Jenniskens, P., Tedesco, E., Murthy, J., Laux, C., Price, S., Spaceborne Ultraviolet 251-384 nm Spectroscopy of a Meteor During the 1997 Leonid Shower, Meteorites and Planetary Science, 37.

Jones, W., 1997. Theoretical and observational determinations of the ionization coefficient of meteors. Mon. Not. R. Astron. Soc. 288, 995-1003.

Lebedinets, V. N., A. V. Manochina and V. B. Shushkova, 1973. Interaction of the lower thermosphere with the solid component of the interplanetary medium. Planet Space Sci. 21, 1317-1332.

C. M. Lisse, K. Dennerl, J. Englhauser, M. Harden, F. E. Marshall, M. J. Mumma, R. Petre, J. P. Pye, M. J. Ricketts, J. Schmitt, J. Trümper, R. G. West, Discovery of X-ray and Extreme Ultraviolet Emission from Comet C/Hyakutake 1996 B2, Science, 274, 5285, 205-209.

Longmire, C. L., Notes on Bebris-air-magnetic Interaction, Rand Corp. Memo, RM-3386-PR.

Love, S. G. and D. E. Brownlee, 1993. A direct measurement of the terrestrial mass accretion rate of cosmic dust. Science, 262, 550-553.

Mathews, J. D., D. Janches, D. D. Meisel, and Q. H. Zhou, 2001. The micrometeoroid mass flux into the upper atmosphere: Arecibo results and a comparison with prior estimates, Geophys. Res. Lett., 28 (10), 1929-1932.

Opik, E. J., 1958. Physics of Meteor Flight in the Atmosphere. Wiley-Interscience, Hoboken, N. J.

Revelle, D. O. , The Mesopause as a Physical Penetration Boundary, J. Atm. Solar-T. Physics, 67, 1159-1170.

Zinn, J, Judd, O. P., and ReVelle D. O. , Leonid Meteor Ablation, Energy Exchange and Trail Morphology, Adv. In Space Res., 33, 1466-1474.

Theoretical and Observational Studies of Meteor Interactions with the Ionosphere

Patrick Colestock, Sigrid Close, John Zinn

Los Alamos NATIONAL LABORATORY EST.1943

LAUR-06-113

The Case for Meteor Studies

- **Dominant contributor to ionospheric metals**
- **Ubiquitous signature in large aperture radar / imaging systems**
- **Primary damage source to space assets**
- **Unique signatures in remote sensing of re-entering objects**

Overview

- Observations of mass flux
- Simplified ablation model
- Plume expansion physics
- Issues to be resolved

Meteors – Radar Scattering

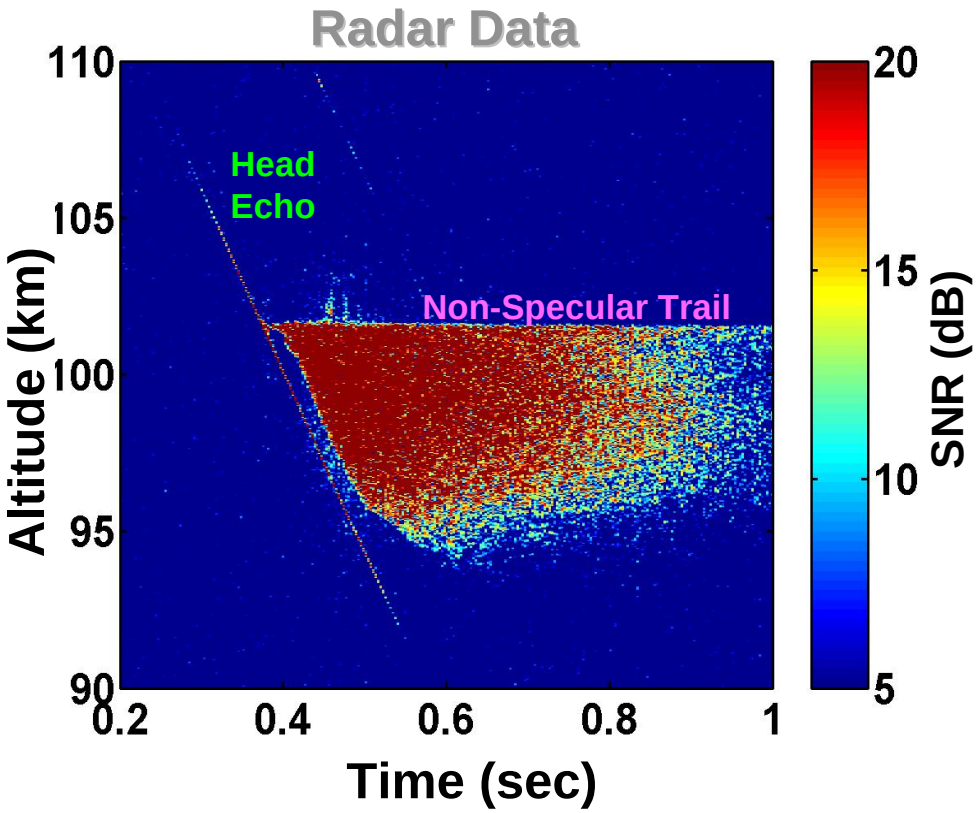

- **Trail**
  - Plasma immediately behind meteoroid
  - Relatively stationary
  - Scattering from field-aligned-irregularities (FAIs)
- **Head Echo**
  - Radar signature of plasma region around meteoroid
  - Moves with velocity of meteoroid
  - Scattering from dense, sphere-like plasma

Los Alamos NATIONAL LABORATORY EST.1943

Example Head Echo Data

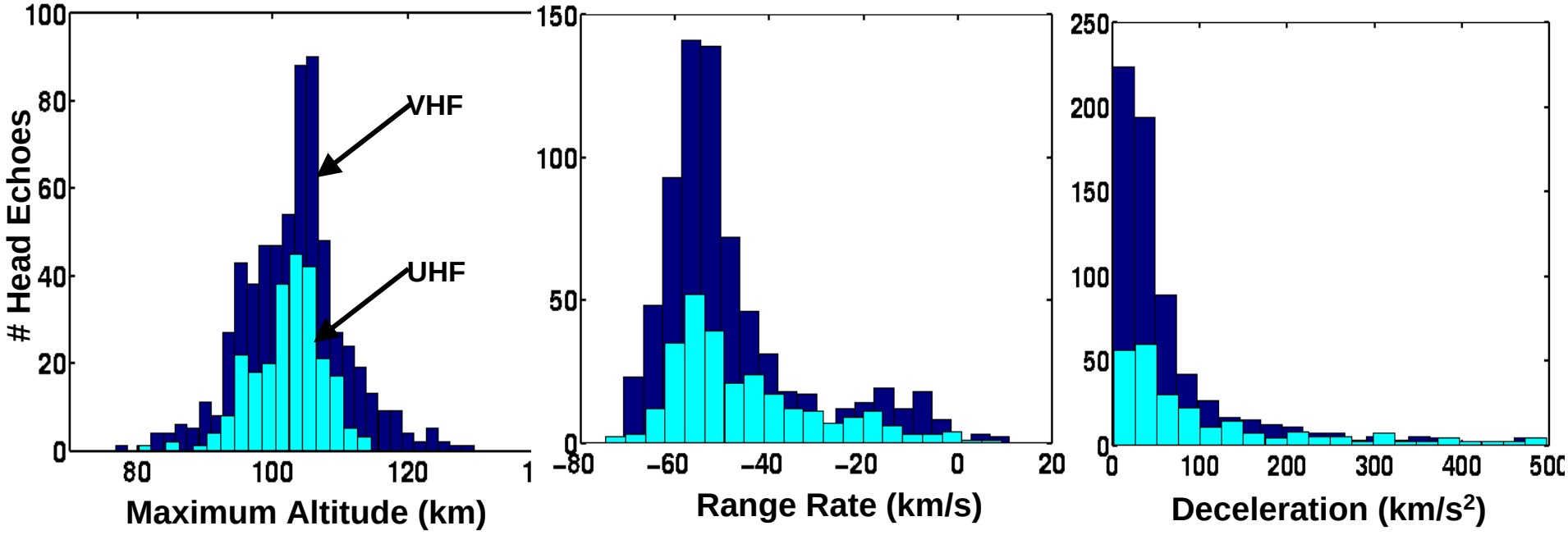

- **Peak altitude near 105 km**
- **Range rate (radial velocity component) histograms are double-peaked**
- **Decelerations typically < 100 km/s²**

Los Alamos NATIONAL LABORATORY EST.1943

Calculating Meteoroid Mass, Radius and Density

- **Mass from new scattering theory**
  - **Convert RCS to plasma density (*n*)**
  - **Convert *n* to electron line density (*q*)**

$$m = \int \frac{q\mu v}{\beta} dt$$

- **Ballistic parameter from deceleration**
  - **Conserve momentum between meteoroid and air**

$$\frac{m}{\pi r^2} = -\frac{(v\gamma\rho \sec\chi)}{dv/dh}$$

- **Density from spherical distribution**

$$\delta = \frac{3m}{4\pi r^3}$$

- **3 equations, 3 unknowns → solve!**

n	Electron density (m^{-3})
q	Electron line density (m^{-1})
μ	Meteoroid molecular mass (gm)
v	Head echo velocity (m/s)
β	Ionization probability
r	Meteoroid radius (m)
γ	Dimensionless drag coefficient
ρ	Air density (gm/m^3)
χ	Angle between path and zenith
h	Head echo altitude (m)
δ	Meteoroid density (gm/m^3)

Meteor Mass Flux Dominated by Low Mass Sporadics

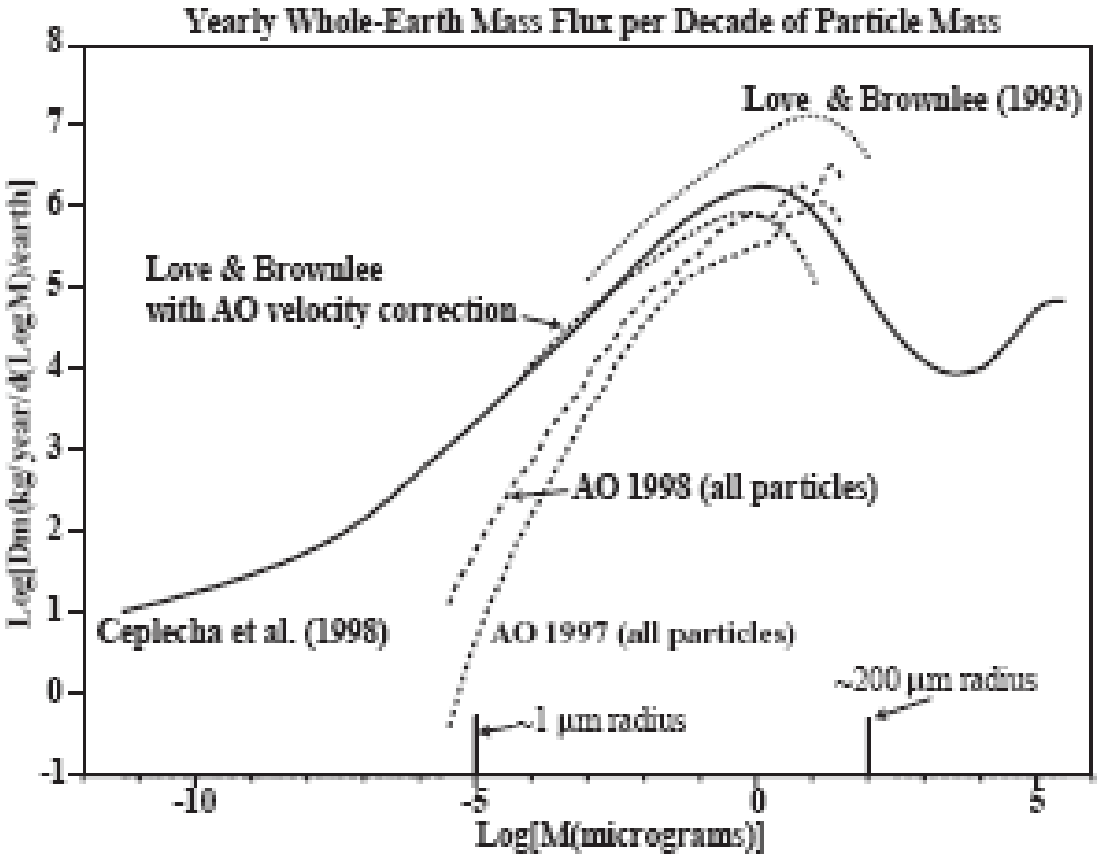

Los Alamos NATIONAL LABORATORY EST.1943

Derived Mass Distributions for Leonids

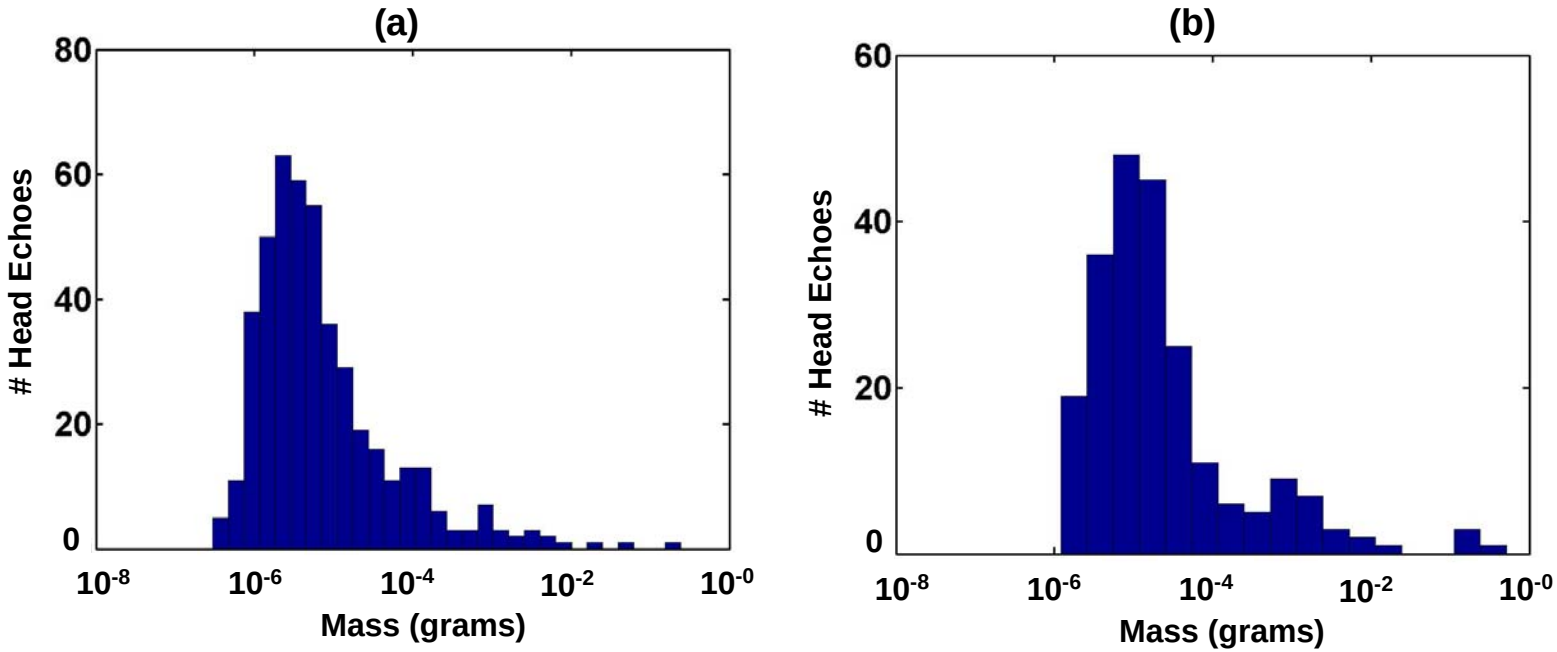

1998 1999

Close, et. al., Icarus, (2004)

Los Alamos NATIONAL LABORATORY EST.1943

Meteor Ablation Model

$$\frac{dm}{dt} = -\frac{1}{2} m_{air} v_0^3 \frac{1}{E_o} S n_{air}$$

Ablation Rate

$$\frac{dm}{ds} = -0.6045 \left(\frac{v_0^2 m_{air} n_{air}}{E_0} \right) \left(\frac{m}{\rho_s} \right)^{2/3}$$

Spherical meteoroid

$$n_{air} = n(z_0) \exp\left\{ -\frac{z - z_0}{H} \right\}$$

Neutral density profile

$$\frac{dm}{dz} = -0.6045 \left(\frac{v_0^2 m_{air} n_{air}(z_0)}{E_0} \right) \frac{m^{2/3}}{\cos\theta} \exp\left\{ -\frac{z - z_0}{H} \right\}$$

Composite ablation equation

Los Alamos NATIONAL LABORATORY EST.1943

Ablation Profiles vs. Altitude for 30 km/sec Meteoroids

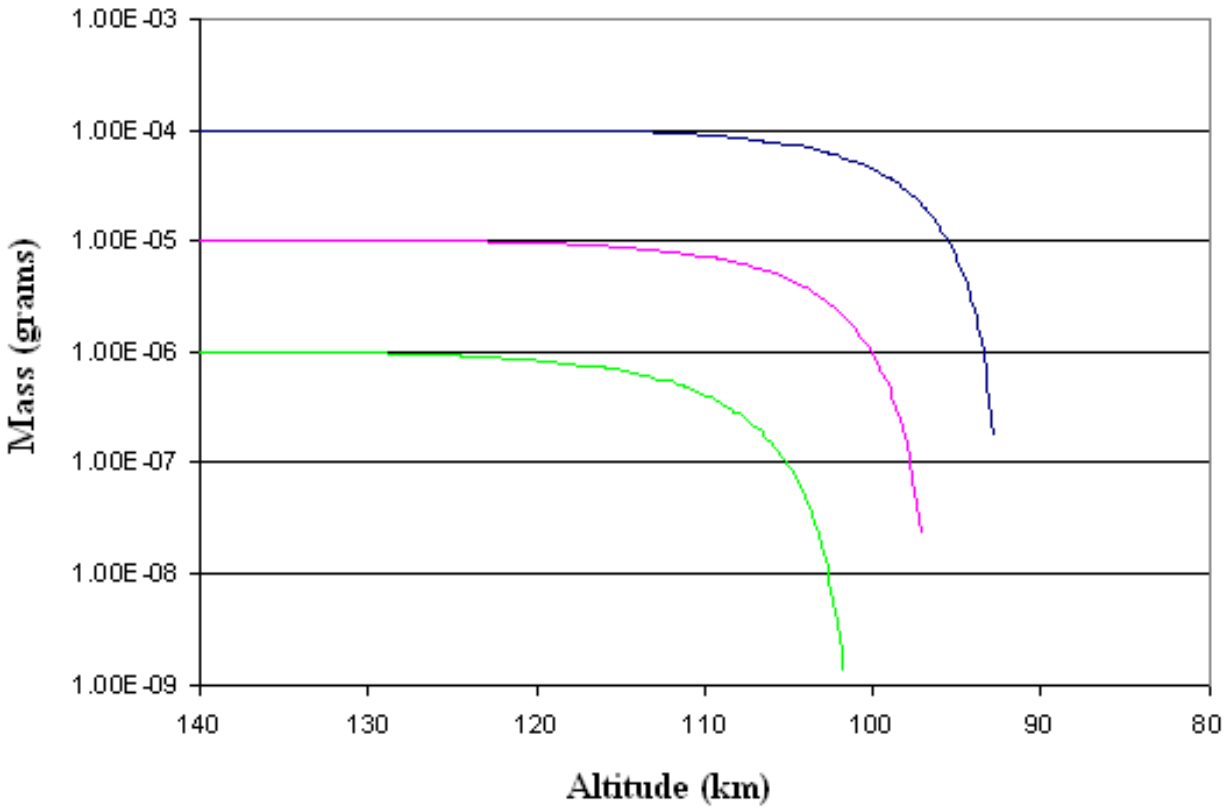

Los Alamos NATIONAL LABORATORY EST.1943

Mass Ablation Rates for 30 km/sec Meteoroids

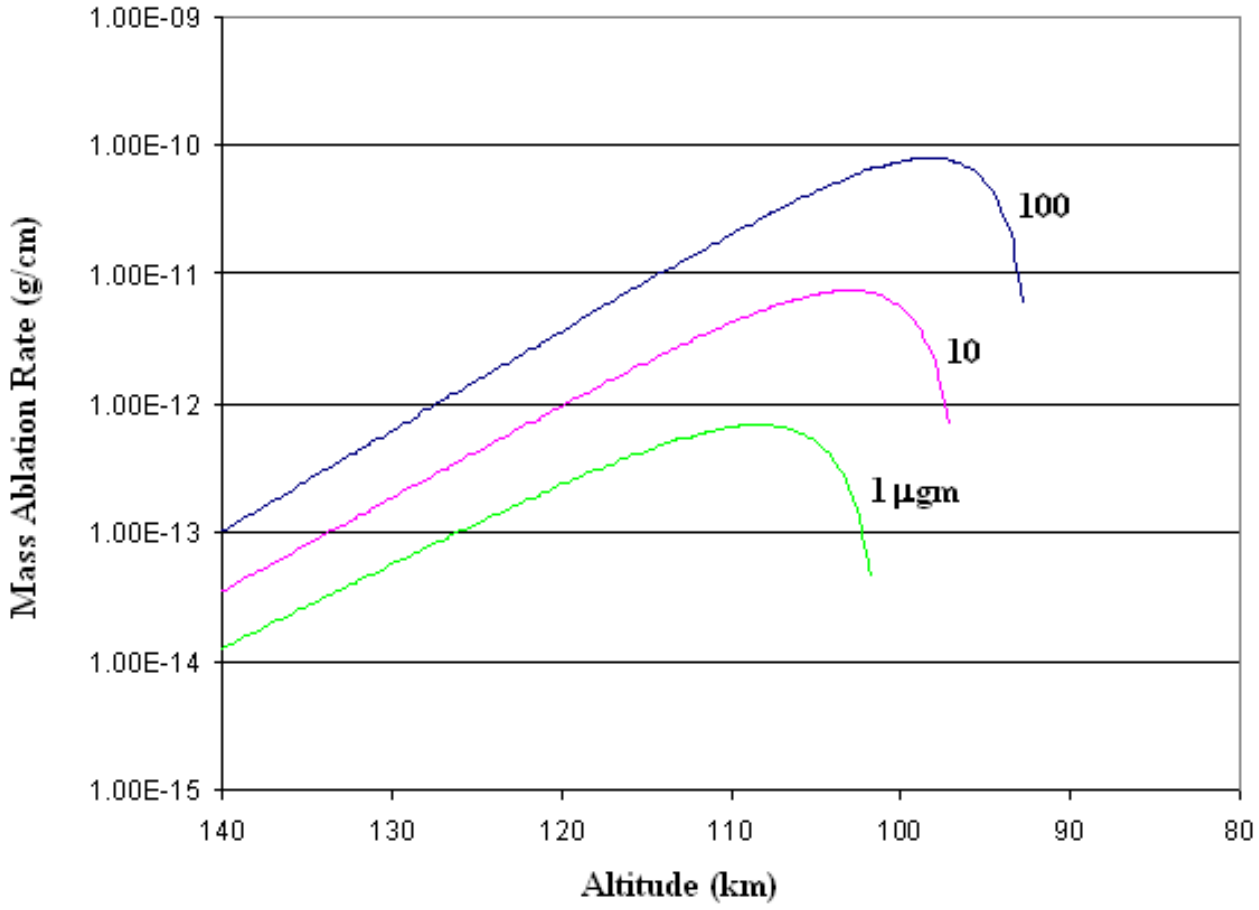

Los Alamos NATIONAL LABORATORY EST.1943

Composite Mass Deposition Profile

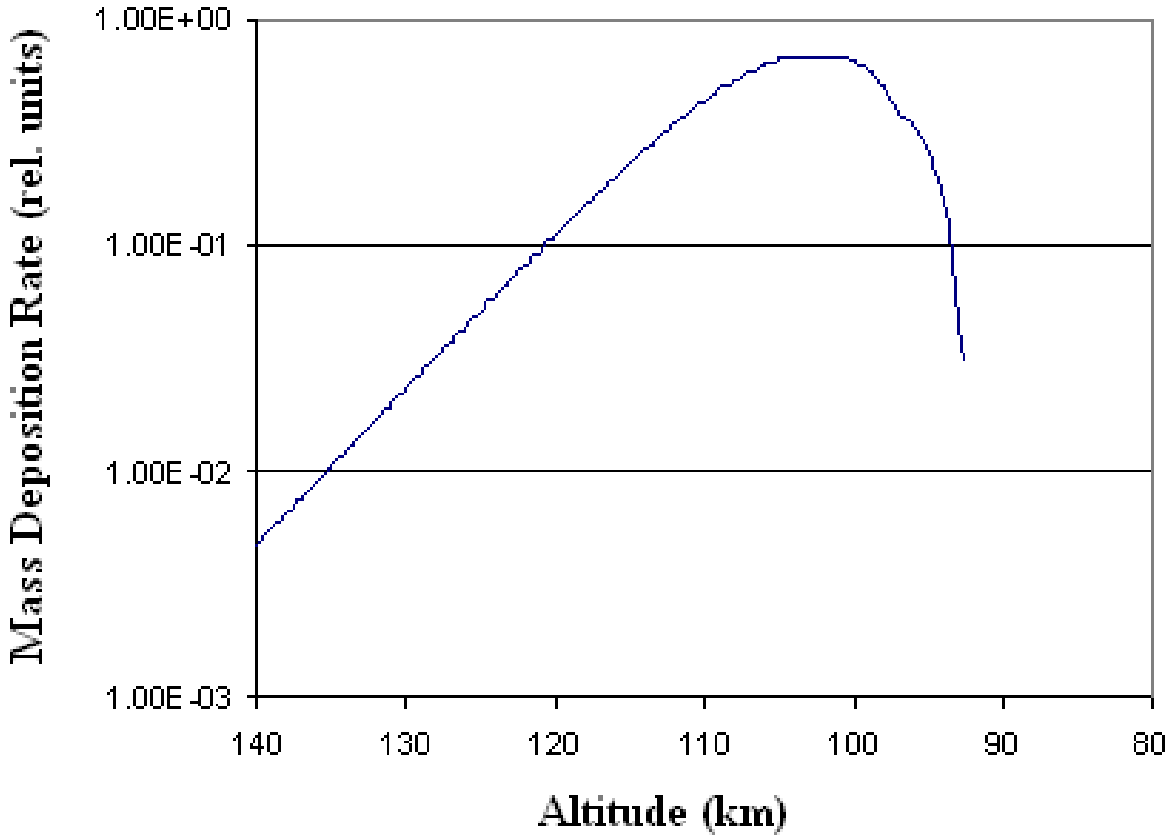

Los Alamos NATIONAL LABORATORY EST.1943

Plasma Plume Regimes

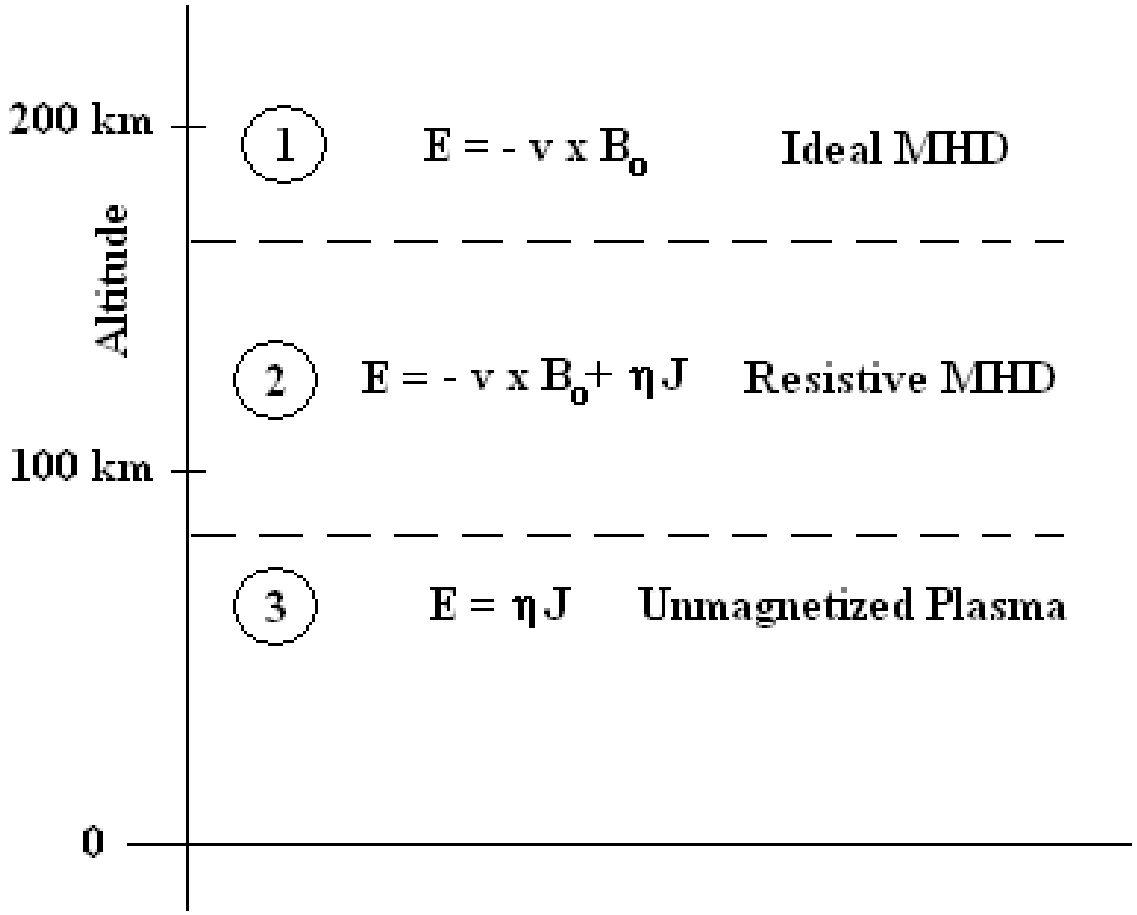

Plasma Expansion around a Meteoroid

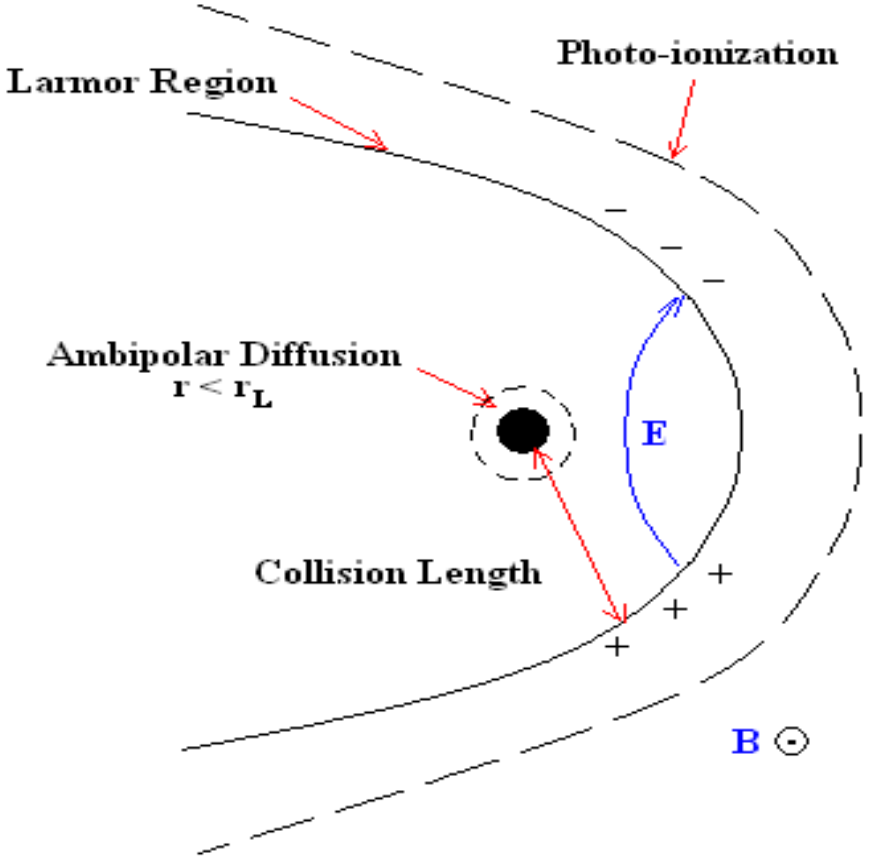

Los Alamos NATIONAL LABORATORY EST.1943

Diamagnetic Bubble Formation

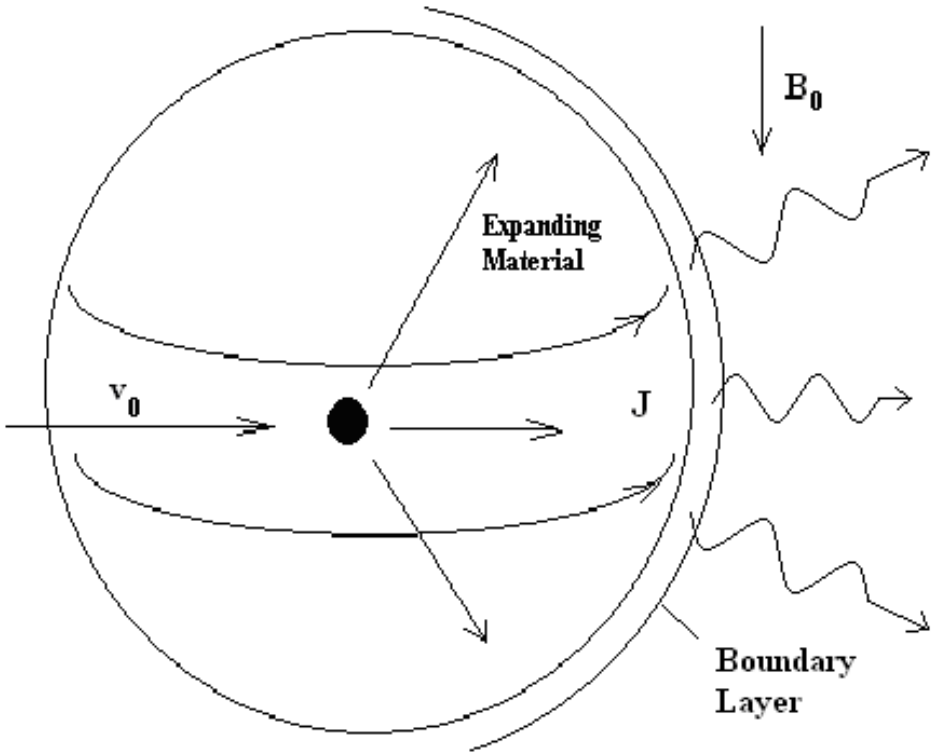

Magnetic Boundary Layer

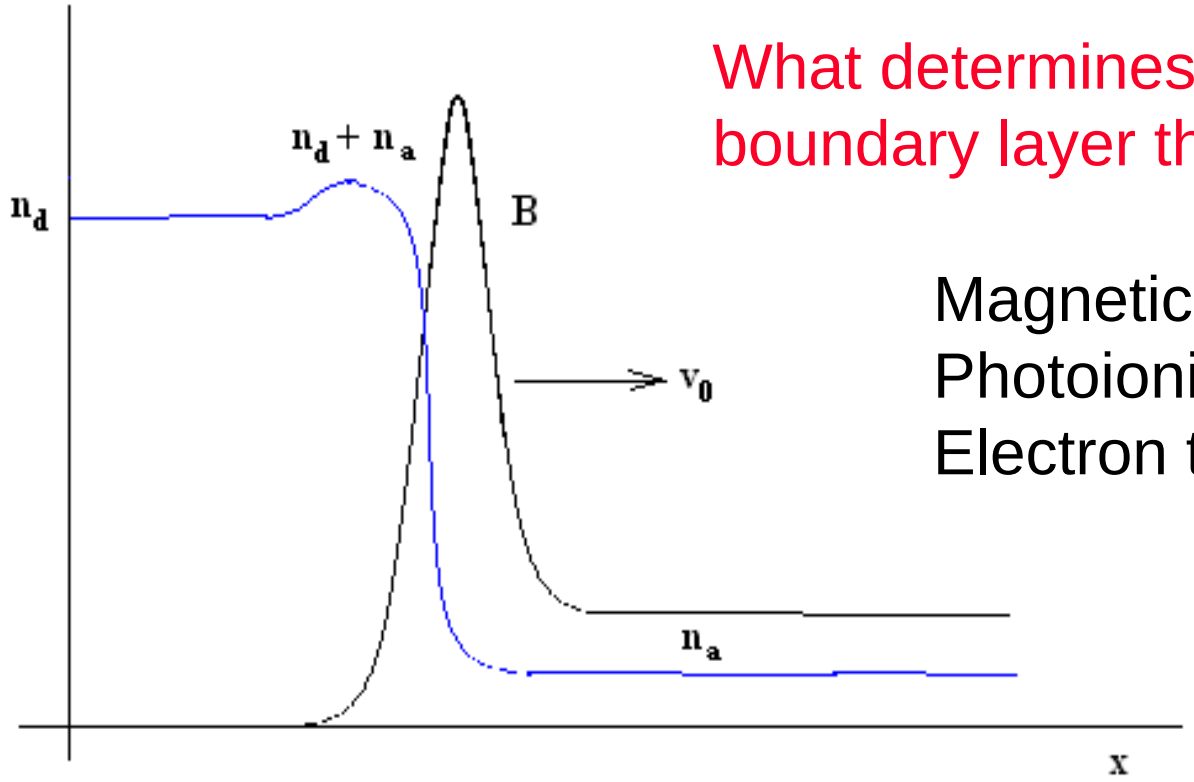

What determines boundary layer thickness?

Magnetic diffusion
Photoionization
Electron temperature

Los Alamos NATIONAL LABORATORY EST.1943

Issues to be Resolved

- **Comprehensive simulation of the meteoroid plasma**
  - **Improved ablation models**
  - **Diamagnetic expansion**
  - **Boundary layer parameters**
- **Improved radar scattering models**
  - **Impact of internal modes**
- **Simulation of optical emission**
  - **Profile effects of energetic emission**
  - **Connection to plasma temperature and/or density**

Meteors and Sprites

- **Meteoric triggering of upper atmospheric transients**

Suszcynsky et al., 1999

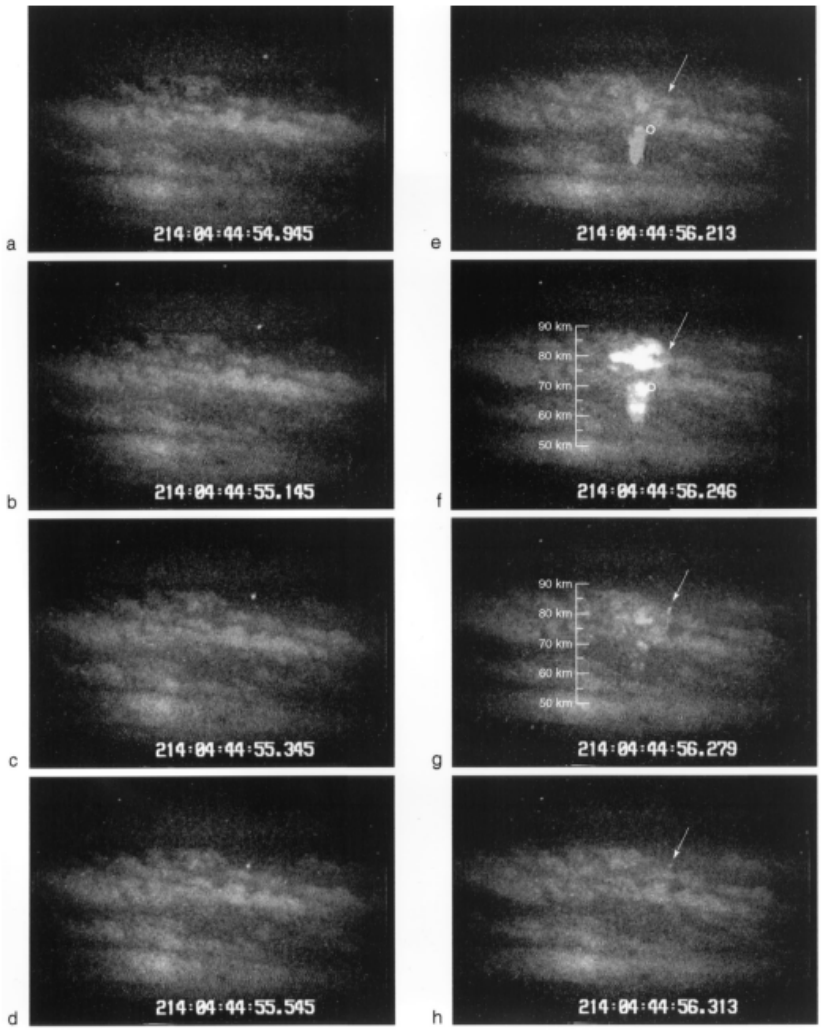

Figure 1. Video frames (33 ms/frame) of the event showing (a–c) the meteor during its trajectory, (d) the meteor just before initial obscuration by foreground clouds, (e) the first frame of the sprite with an arrow indicating the observed trajectory of the meteor and a circle indicating the position of the meteor at the time of the sprite, assuming that it continued to travel behind the foreground clouds at a constant velocity, (f) the second frame of the sprite showing an altitude scale and the same arrow and circle as in Figure 1e, (g) the third frame of the sprite and first frame of the jet with altitude scale and an arrow indicating the general path direction of the meteor, and (h) the second frame of the jet showing the same arrow as in Figure 1g.